Biomacromolecules

pubs.acs.org/Biomac

Article

Squid Beak Inspired Cross-Linked Cellulose Nanocrystal Composites

Yefei Zhang, Nanetta Pon, Ahmed Awaji, and Stuart J. Rowan*

Cite This: *Biomacromolecules* 2021, 22, 201−212

Read Online

ACCESS | Metrics & More | Article Recommendations | Supporting Information

ABSTRACT: Bioinspired cross-linked polymer nanocomposites that mimic the water-enhanced mechanical gradient properties of the squid beak have been prepared by embedding either carboxylic acid- or allyl-functionalized cellulose nanocrystals (CNC) into an alkene-containing polymer matrix (poly(vinyl acetate-*co*-vinyl pentenoate), P(VAc-*co*-VP)). Cross-linking is achieved by imbibing the composite with a tetrathiol cross-linker and carrying out a photoinduced thiol−ene reaction. Central to this study was an investigation on how the placement of cross-links (i.e., within matrix only or between the matrix and filler) impacts the wet mechanical properties of these materials. Through cross-linking both the CNCs and matrix, it is possible to access larger wet mechanical contrasts (E'_{stiff}/E'_{soft} = ca. 20) than can be obtained by just cross-linking the matrix alone (where contrast E'_{stiff}/E'_{soft} of up 11 are observed). For example, in nanocomposites fabricated with 15 wt % of allyl-functionalized tunicate CNCs and P(VAc-*co*-VP) with about 30 mol % of the alkene-containing VP units, an increase in the modulus of the wet composite from about 14 MPa to about 289 MPa at physiological temperature (37 °C) can be observed after UV irradiation. The water swelling of the nanocomposites is greatly reduced in the cross-linked materials as a result of the thiol−ene cross-linking network, which also contributes to the wet modulus increase. Given the mechanical turnability and the relatively simple approach that also allows photopatterning the material properties, these water-activated bioinspired nanocomposites have potential uses in a broad range of biomedical applications, such as mechanically compliant intracortical microelectrodes.

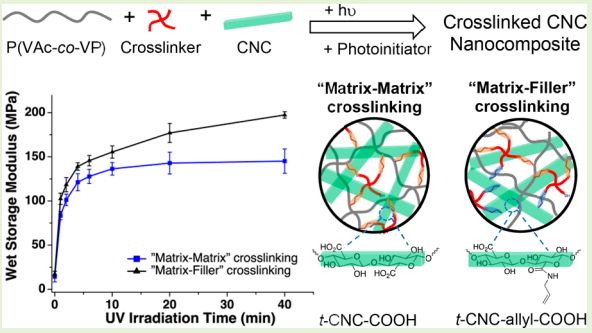

INTRODUCTION

Polymer nanocomposites that consist of nanosized fillers embedded within a polymer matrix are frequently utilized in natural systems to create biological materials with a broad range of exceptional physical properties.[1−4] Examples of biological nanocomposites include nacre, which demonstrates remarkable toughness,[5] the dermis of the sea cucumber, which shows mechanical adaptability,[6−8] and the club of the mantis shrimp, which exhibits exceptional damage tolerance.[9,10] Understanding the mechanism of such biological systems allows for the development of new composites that either directly mimic the function and properties of natural materials or employs nature's design strategies to enhance the performance of synthetic systems.[11−17] Such bioinspired nanocomposites have already been designed and used in a number of applications, such as structural materials,[18−21] functional coatings,[22] intracortical sensors,[23] and energy-harvesting membranes.[24]

The beak of the Humboldt squid is another interesting example of a biological composite that consists of chitin nanofibers embedded in a protein matrix. In this case, the beak displays a water-enhanced mechanical gradient that spans 2 orders of magnitude in stiffness to seamlessly join the stiff tip of the beak (rostrum, elastic modulus 5 GPa) to the squid's soft muscle tissues (buccal, elastic modulus 50 MPa).[25,26] The excellent mechanical gradient properties of the beak are achieved by changes in the degree of covalent cross-linking and water hydration between the stiff rostrum and the soft buccal base.[27] The soft buccal region is mainly composed of water-hydrated chitin (ca. 80 wt % water) with a small percent of chitin-binding proteins (DgCBPs). Moving closer to the rostrum region, the water is gradually replaced with hydrophobic histidine-rich proteins (DgHBPs), which after cross-linking (via histidine groups and catechol moieties from both low molecular weight and peptidyl catechol compounds) results in a cross-linked protein network that interpenetrates the chitin filler network.[28−30] It is worth pointing out that, in a dehydrated squid beak (i.e., not a natural environment for the squid), the 100-fold mechanical gradient between the rostrum and buccal regions is greatly diminished (modulus ranging from 10 to 5 GPa).

The better understanding of the squid beak (and other examples of mechanical gradient systems in nature) as a

Special Issue: Bioinspired Macromolecular Materials

Received: July 12, 2020
Revised: September 10, 2020
Published: September 24, 2020

https://dx.doi.org/10.1021/acs.biomac.0c01051
Biomacromolecules 2021, 22, 201−212

material has led to increased interest in new bioinspired synthetic materials[11,22,31−34] which, for example, could serve as modulus buffers that can bridge soft tissue and stiff implants in some biomedical engineering applications, such as orthopedic implants[35,36] and intracortical microelectrodes.[23,37,38] For example, the lifetime of the current silicon-based intracortical microelectrodes is limited by the chronic inflammatory response of the brain. It has been suggested that this response is, at least in part, a result of the large mechanical mismatch between the stiff electrode and the soft brain tissue.[39] In prior work it has been shown that CNC-based composite films, which are stiff for implantation, soften once inserted into the brain, resulting in a reduced inflammatory response.[23,37] The ability to access such materials with a mechanical gradient would allow access to probes that transition from the desired lower modulus at the tissue interface to a higher modulus for device interfacing.

However, there is still a noticeable gap between the engineered composites and the biological materials with regard to the mechanical contrast and the stiff modulus when the material is wet. Rolandi and co-workers reported the fabrication of chitosan nanocomposites with tunable mechanical properties by controlling the degree of cross-linking chitosan with L-3,4-dihydrophenyl-alanine (L-dopa) through an oxidation reaction initiated by sodium periodate.[31] However, the gradient and stiff modulus in these hydrated samples are relatively low (elastic modulus from 26 to 55 MPa) compared to the squid beak biomodel. To date, the largest mechanical contrast observed in synthetic materials has been reported by Guan and co-workers who, inspired by the jaw of the polychaete worm, used imidazole-containing polymer networks cross-linked by metal ions.[32] The degree of cross-linking was controlled by varying the concentration of metal ions, which resulted in a gradient that spans across 0.5 to 100 MPa in dry low T_g films.

In prior work we have reported bioinspired mechanically adaptive polymer nanocomposites that have been designed to mimic the hydration-enhanced mechanical gradient behavior of the squid beak.[40,41] By embedding allyl-functionalized cellulose nanocrystals (CNC) into a poly(vinyl acetate) (PVAc) matrix, along with a tetrathiol cross-linker (pentaerythritol tetrakis(3-mercaptopropionate), PETMP), the CNC fillers can be covalently cross-linked via photoinduced thiol−ene chemistry, and the degree of cross-linking can be controlled by UV irradiation exposure. In the dry state, hydrogen bonding interactions between the CNC fillers and between the filler and matrix result in a significant increase in the mechanical properties of the composites. However, in the hydrated state, the modulus of the un-cross-linked composites drops dramatically (to <20 MPa) on account of disruption of the hydrogen bonding between the CNCs (and CNCs and matrix) by the water molecules, as well as water plasticization of the polymer matrix. However, covalent cross-linking between the CNCs reduces the degree of water softening, yielding a wet modulus of about 130 MPa at maximum degree of cross-linking. As such, it was possible to obtain water-activated mechanical gradients with a wet modulus contrast, E'_{stiff}/E'_{soft}, of about 7 between cross-linked and un-cross-linked materials.[41]

While this initial study showed that it was possible to access water-activated mechanical gradients in CNC composites, the wet mechanical contrast achieved in these first-generation bioinspired nanocomposites is still far away from the gradient observed in squid beak materials (E'_{stiff}/E'_{soft} ca. 7 vs 100). For many applications it is important to be able to access modulus gradients that span across larger mechanical contrasts while at the same time being able to access stiffer wet films (larger E'_{stiff}). As such, it is of interest to investigate different approaches in materials design and cross-linking strategies to further improve this class of bioinspired nanocomposites. One possible route is to introduce matrix−matrix and CNC−matrix cross-links (which have been shown to improve the mechanical stiffness of CNC-based nanocomposites[42−44]) instead of the CNC−CNC only cross-links used in the prior study. In fact, the impressive wet stiffness in the rostrum area of the squid beak is achieved through a densely cross-linked protein matrix. Furthermore, a much higher mol % of alkene cross-linking groups can be incorporated into the matrix than is possible through functionalization of the nanofiller, which should result in much higher degrees of cross-linking and therefore wet stiffness. As such, reported herein are investigations of two types of thiol−ene cross-linkable CNC nanocomposites (Scheme 1), one where cross-linking occurs primarily within

Scheme 1. Schematic of the Preparation of Bio-Inspired Nanocomposites Based on Matrix−Matrix Cross-Link and Matrix−Filler Cross-Link Approaches

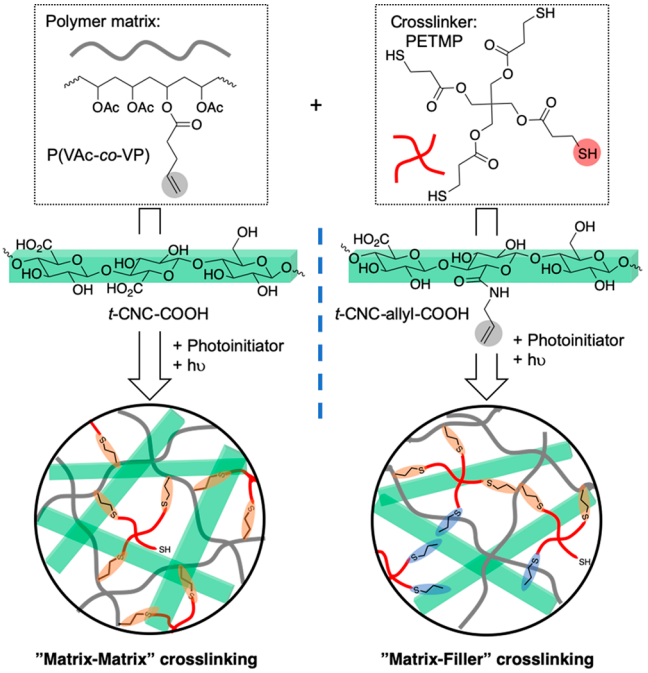

the polymer matrix and one where cross-linking can occur between matrix and CNCs (in addition to within the matrix and between the CNCs themselves). The goal here is to better mimic the wet mechanical contrast of the squid beak and develop a better understanding of this class of bioinspired composites. In addition, the possibility of photopatterning of these nanocomposites is explored to access water-activated shape-changing films.

EXPERIMENTAL SECTION

Materials. Oxalyl chloride, 4-(dimethylamino)pyridine (DMAP), 4-pentenoic acid, triethylamine phenylbis(2,4,6-trimethylbenzoyl)-phosphine oxide (BAPO), pentaerythritol tetrakis(3-mercaptopropionate) (PETMP), and poly(vinyl acetate) (PVAc, M_w = 100000 g/mol) were purchased from Sigma-Aldrich and used as received.

https://dx.doi.org/10.1021/acs.biomac.0c01051
Biomacromolecules 2021, 22, 201−212

Hydrochloric acid, sodium bicarbonate, and all solvents were purchased from Fisher Scientific and used without further purification. TEMPO-oxidized cellulose nanocrystals (*t*-CNC-COOH) with a charge density of 1000 mmol/kg, allyl-functionalized cellulose nanocrystals (*t*-CNC-allyl-COOH) with an allyl functionality of 800 mmol/kg and a residual charge density of 200 mmol/kg were obtained from sea tunicate mantles using the procedures published in previous work.[40,41]

Synthesis of Poly(vinyl acetate-*co*-vinyl alcohol) P(VAc-*co*-VA). P(VAc-*co*-VA) copolymers were prepared by partial hydrolysis of PVAc under acidic conditions. PVAc (15 g, M_w = 100000 g/mol) dissolved in a 9:1 (v/v) methanol/water mixture (250 mL) was heated to 50 °C for 1 h. 12 M HCl is added to the reaction mixture until the concentration of the HCl is 0.2 M (ca. 4.2 mL), and the hydrolysis reaction was carried out for 2, 4, or 6 h at 50 °C. After the reaction, the solution was concentrated to about 50 mL and precipitated in excess DI water. The product was rinsed with DI water, redissolved in 50 mL of methanol and reprecipitated in water. The degree of hydrolysis of the P(VAc-*co*-VA_x) (where x is 10, 21, or 29 corresponding to the mole fraction of VA units) was calculated via ^{1}H NMR peak integration (see Supporting Information).

Synthesis of 4-Pentenoyl Chloride. To a solution of 4-pentenoic acid (10.01 g, 100 mmol) in 150 mL of anhydrous dichloromethane (DCM) was added oxalyl chloride (13.96 g, 110 mmol) and one drop of anhydrous dimethylformamide (DMF). The reaction was stirred for 6 h at room temperature. Excess solvent was fully removed by rotary evaporation at 40 °C. The resulting 4-pentenoyl chloride product was confirmed by NMR (Figure S3) and used without further purification (yield 95%).

Synthesis of Poly(vinyl acetate-*co*-vinyl pentenoate) P(VAc-*co*-VP). Sample procedure for the synthesis of P(VAc-*co*-VP_{10}) copolymer: P(VAc-*co*-VA_{10}) (5 g, 6.11 mmol of OH groups) was dissolved in 200 mL of anhydrous tetrahydrofuran (THF). DMAP (0.07 g, 0.61 mmol) and triethylamine (3.09 g, 30.56 mmol) were dissolved in anhydrous THF separately and transferred to the reaction under argon. The reaction vessel was placed in an ice bath and cooled before 4-pentenoyl chloride (1.45 g, 12.23 mmol) in 25 mL of THF was added dropwise over 30 min. The reaction was then allowed to continue for 3 h at room temperature followed by 16 h at 60 °C. The THF was fully removed by rotary evaporation, and the products were redissolved in ethyl acetate (EtOAc). The mixture was washed with saturated sodium bicarbonate solution (5×), followed with 0.1 M HCl solution (5×), and finally with DI water (5×). The product was further purified by dissolving in THF and passing through a silica packed column. Finally, the purified polymer was precipitated in hexane and dried in a vacuum oven. ^{1}H NMR spectra of the copolymer in $CDCl_3$ is shown in Figure S4. A new peak appeared between 5.6 and 5.9 ppm corresponding to the alkene group's internal proton (-C**H**=CH_2) in the VP units. The mole fraction of VP units was characterized by NMR integration (see Supporting Information). Similar procedures were carried out for the synthesis of P(VAc-*co*-VP_{22}) and P(VAc-*co*-VP_{30}) by using P(VAc-*co*-VA_{21}) (5 g, 12.89 mmol of OH) and P(VAc-*co*-VA_{29}) (5 g, 20.44 mmol of OH), respectively. The isolated yield of the esterification reactions was all above about 75%.

Fabrication of *t*-CNC/P(VAc-*co*-VP) Nanocomposites. *t*-CNC-COOH/P(VAc-*co*-VP_x) and *t*-CNC-allyl-COOH/P(VAc-*co*-VP_x) nanocomposites with different mole percent VP were prepared by solution casting from DMF. For a target nanocomposite containing 15 wt % of CNC fillers, 510 mg of P(VAc-*co*-VP_x) (x = 10, 22, and 30) was dissolved in DMF at 50 mg/mL by stirring at room temperature for 4 h, and 90 mg of *t*-CNC−COOH or *t*-CNC-allyl-COOH was homogeneously dispersed in DMF at 3 mg/mL via ultrasonication for 30 min. The nanocomposites were prepared by mixing the polymer solution with the CNC dispersion and submitting to ultrasonication for about 30 min before casting into a PTFE dish (diameter 12 cm). The solvent was fully removed in a vacuum oven at 60 °C for 5 days. Thermogravimetric analysis (TGA) was used to confirm the removal of DMF. The dried nanocomposite films were removed from the PTFE dishes and used as-cast without any melt processing.

Imbibing Process. Dried nanocomposite films were cut into rectangular strips with approximate dimensions of 30 mm by 4 mm. Stock solutions of the photoinitiator (phenylbis(2,4,6-trimethylbenzoyl)phosphine oxide, BAPO; 5 mM) and cross-linker (pentaerythritol tetrakis(3-mercaptopropionate), PETMP; 50 mM) were prepared by dissolving the reagents in DCM separately. The exact volume of stock solution of initiator and cross-linker were measured (initiator, 5 mol % with respect to alkene groups, and cross-linker, 25 mol % with respect to alkene groups, calculated with reference to the molar amount of total alkene groups from both CNCs and polymer matrix) and combined, and the cosolution was slowly and evenly pipetted onto the film until the solution was absorbed. The imbibed films were then supported on a PTFE dish and annealed in saturated DCM vapor for 24 h with the exclusion of light, with the goal of ensuring a more homogeneous distribution of the photoinitiators and cross-linkers within the film. Finally, the film strips were carefully dried in a dark environment under reduced pressure for 24 h to remove any residual DCM.

Photo Cross-Linking Process. UV-induced thiol−ene cross-linking was performed using a Honle Bluepoint UV source with an intensity of 60 mW/cm^2 measured in the wavelength interval 320 to 390 nm. Composite films supported on a piece of Teflon film were placed on a hot plate set at 60 °C before being irradiated for different times ranging from 2 to 40 min. Each sample was turned over at half of the exposure time to expose both sides to the UV irradiation. The irradiated films were soaked in 2-propanol immediately after exposure in order to remove any unreacted initiator and cross-linker. The 2-propanol was refreshed three times during a 24 h soaking period. Finally, the samples were removed from 2-propanol and allowed to dry in a well-ventilated hood overnight before the removal of any residual solvent under reduced pressure at 40 °C for 48 h.

Characterization. *Nuclear Magnetic Resonance (NMR) Spectroscopy.* ^{1}H NMR measurements were performed using a Bruker Avance II 500 spectrometer operating at 500 MHz. Spectra are collected at room temperature with a minimum of 16 scans. Spectra were calibrated to the residual solvent peak of $CDCl_3$ (7.26 ppm ^{1}H NMR). Data were treated with MNova software.

Fourier Transform Infrared Spectroscopy (FTIR). FTIR studies of nanocomposite films were performed using a Shimadzu IRTracer-100 FTIR spectrometer. Film samples were placed directly on the ATR crystal, and the spectra were collected in transmission mode between 400 to 4000 cm^{-1} with a resolution of 4 cm^{-1}.

Differential Scanning Calorimetry (DSC). DSC measurements were performed using a TA Instruments Discovery DSC 2500. All samples were first heated to 100 °C and cooled down to −20 °C at a rate of 10 °C min^{-1}. And then the samples were heated back up again from −20 to 100 °C at a rate of 10 °C min^{-1}. The second heating cycle was used for data analysis.

Water Swelling. Swelling tests were performed by placing the composite samples into vials filled with DI water and left in a water bath at 45 °C for 48 h. The degree of swelling was calculated by

$$\%\text{swelling} = \frac{\text{wet mass} - \text{dry mass}}{\text{dry mass}} \times 100$$

Dynamic Mechanical Analysis (DMA). The viscoelastic properties of nanocomposites were analyzed using a RSA-G2 solid analyzer (TA Instrument, DE) equipped with a tension clamp and a submersion chamber. Dynamic temperature sweep measurements were performed with a fixed frequency of 1 Hz, a strain of 0.1%, a preload force of 0.1 N, and 125% force track. For characterizing the dry modulus of the composite films, the tension clamp was used and the modulus was measured while the temperature increased from 0 to 100 °C at a heating rate of 3 °C min^{-1}. The wet modulus was measured using the submersion chamber which allows the measurements to be conducted while the films were fully immersed in water during the tests. The temperature of the water was increased from 17 to 50 °C at a heating rate of 3 °C min^{-1}. It is worth pointing out that in the case of the submersion test, all samples were preswollen in water for 48 h before

https://dx.doi.org/10.1021/acs.biomac.0c01051
Biomacromolecules 2021, 22, 201−212

the test. All the DMA tests were performed in triplicate and the standard deviations were plotted as error bars.

RESULTS AND DISCUSSION

Synthesis and Characterization of P(VAc-*co*-VP). As the initial work discussed above focused on using poly(vinyl acetate), PVAc, as the polymer matrix it was decided to target poly(vinyl acetate-*co*-vinyl pentenoate) (PVAc-*co*-VP), with various amounts of vinyl pentanoate repeat units, as the thiol−ene cross-linkable matrix. As such, commercially available PVAc was partially hydrolyzed to poly(vinyl acetate-*co*-vinyl alcohol) (P(VAc-*co*-VA)) using acidic conditions (Scheme 2a), as it has been reported that this allows for good control of the degree of hydrolysis and results in a copolymer whose VA repeat units are randomly distributed along the polymer backbone.[45,46] The degree of hydrolysis was controlled by varying the reaction time to target copolymers with about 10 mol %, 20 mol %, and 30 mol % of VA units.[47] The final degree of hydrolysis was estimated by ^{1}H NMR (Figure S1) to be 10%, 21%, and 29% for PVAc hydrolyzed for 2, 4, and 6 h, respectively (Table S1). Furthermore, after partial hydrolysis of PVAc, a new peak appeared in the FTIR spectra at 3300 cm^{-1} corresponding to the −OH groups of the P(VAc-*co*-VA) copolymer (Figure S2).

Poly(vinyl acetate-*co*-vinyl pentenoate) (P(VAc-*co*-VP)) copolymers were then prepared by the esterification of the hydroxyl groups of the different P(VAc-*co*-VA)s with 4-pentenoyl chloride (Scheme 2a). The molar fraction of VP units on the polymer can be calculated via ^{1}H NMR (Figure S4) to be about 10, 22, and 30%, as shown in Table S2 (P(VAc-*co*-VP$_x$), where x, which corresponds to the mole fraction percent of VP units, is 10, 22, or 30). Conversion of the VA units to VP units was also confirmed by FTIR (Figure S2), as the −OH peak at 3300 cm^{-1} disappeared after esterification and new peaks at 920 cm^{-1} (=C−H) and 1647 cm^{-1} (C=C) appear. The glass transition temperature (T_g) of the copolymers was investigated by DSC. All P(VAc-*co*-VP$_x$) copolymers showed a single glass transition temperature that decreases with increasing percentage of VP units (Figure S5). The measured T_gs are close to the values calculated via the Fox eq (Table S2), consistent with a random distribution of VP units along the polymer backbone.

Scheme 2. Synthesis of (a) Poly(vinyl acetate-*co*-vinyl pentenoate), P(VAc-*co*-VP), in Two Steps from Poly(vinyl acetate), PVAc, and (b) Allyl-Functionalized CNCs (*t*-CNC-allyl-COOH) from Carboxylic Acid-Functionalized CNCs (*t*-CNC-COOH)

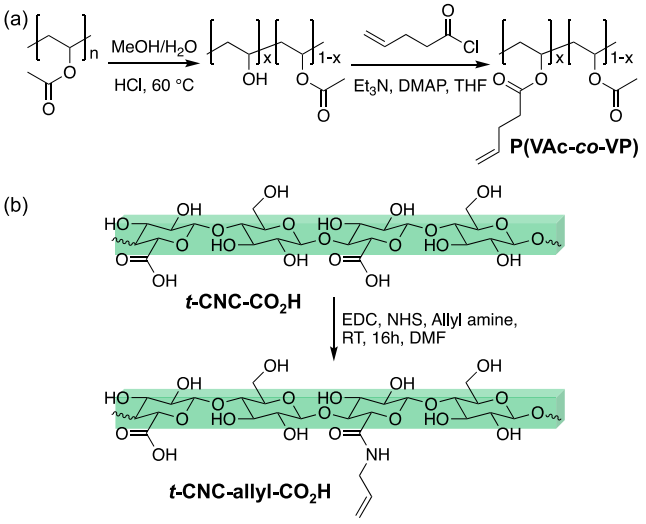

Nanocomposites with Only Cross-Linked Polymer Matrix. As mentioned above, prior work on the first-generation of these bioinspired composites focused on understanding the effect of only cross-linking the CNC nanofiller.[40,41] However, cross-linking of the protein matrix is a critical feature of the squid beak biomodel.[25] In addition, the placement of the alkene moiety in the matrix polymer dramatically increases the potential number of cross-linking sites in the composite. For example, in the first generation, 15 wt % *t*-CNC-allyl-COOH/PVAc composites the amount of alkene units in the film corresponds to about 0.12 × 10^{-3} mmol/mg. However, the use of the P(VAc-*co*-VP$_x$) matrix with 15 wt % *t*-CNC-COOH results in composites that contain an order of magnitude higher concentration of alkene moieties, namely, 0.94 × 10^{-3}, 1.99 × 10^{-3}, and 2.60 × 10^{-3} mmol/mg alkene moieties for x = 10, 22, and 30, respectively. Thus, a series of materials were prepared to examine how cross-linking only the matrix with these much higher levels of potential cross-linking sites would impact the properties of these bioinspired synthetic films. To this end, *t*-CNC-COOHs (with no alkene units attached) were embedded into the three different P(VAc-*co*-VP$_x$) copolymer matrices. These nano-

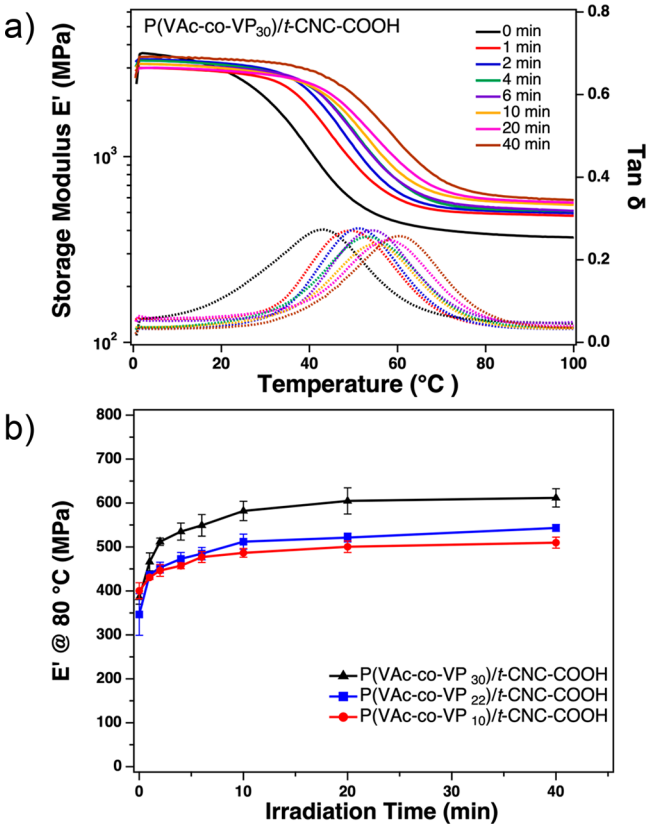

Figure 1. (a) Representative DMA temperature sweep study of P(VAc-*co*-VP$_{30}$)/*t*-CNC-COOH nanocomposites in the dry state before and after UV irradiation. (b) Storage modulus, E', at 80 °C of various P(VAc-*co*-VP)/*t*-CNC-COOH nanocomposites after different UV irradiation times (N = 3, error bars represent the standard deviation; DMA conditions: heating rate 3 °C/min, frequency 1 Hz, strain 0.1%).

https://dx.doi.org/10.1021/acs.biomac.0c01051
Biomacromolecules 2021, 22, 201−212

Table 1. Summary of the Thermal Mechanical Property of P(VAc-*co*-VP_{30})/*t*-CNC-COOH in Both Dry and Wet State at Different UV Irradiation Times (N = 3, Errors are Standard Deviation)[a]

	P(VAc-*co*-VP_{30})/*t*-CNC-COOH				
irradiation time (min)	dry E' at 80 °C (MPa)	dry T_g (°C)	wet E' at 50 °C (MPa)	wet T_g (°C)	water swelling (%)
0	385 ± 15	43.4 ± 1.1	13 ± 5		86 ± 3.5
1	466 ± 20	51.2 ± 2.4	83 ± 5	25.4 ± 0.6	7 ± 2
2	512 ± 8	51.6 ± 0.6	101 ± 7	27.9 ± 0.7	6.5 ± 1
4	535 ± 19	52.0 ± 1.9	120 ± 10	28.1 ± 0.4	6 ± 0.9
6	549 ± 25	53.2 ± 2.3	130 ± 8	28.6 ± 0.3	5.8 ± 0.9
10	582 ± 22	54.0 ± 4.1	136 ± 7	29.3 ± 0.9	5.6 ± 1.0
20	605 ± 30	55.3 ± 2.6	143 ± 12	29.7 ± 0.2	5.5 ± 1.0
40	612 ± 21	57.6 ± 3.4	145 ± 14	30.2 ± 0.2	5.3 ± 0.7

[a]All data are based on DMA experiments.

composites were fabricated by mixing a DMF solution of the polymer and a dispersion of the *t*-CNC-COOHs in DMF. After solution casting and solvent evaporation, optically clear composite films with a thickness between 100 and 120 μm were obtained. In the prior studies it was shown that melt processing of the CNC composites can induce phase segregation which disrupts the CNC filler network and negatively impacts the mechanical properties.[41] Therefore, all the composite films fabricated in this study were used as-cast without any melt processing. The nanocomposites were subsequently imbibed with a tetra-thiol cross-linker, pentaerythritol tetrakis(3-mercaptopropionate) (PETMP), and a photoinitiator, phenylbis(2,4,6-trimethylbenzoyl)phosphine oxide (BAPO), in order to form thiol−ene cross-links upon UV irradiation. It is worth pointing out that in each composite sample the imbibed amount of PETMP cross-linker was adjusted based on the total amount of alkene groups within the polymer matrix to maintain a constant 1:1 thiol to alkene mole ratio. Exposure of these films to UV irradiation results in cross-linking, which was initially confirmed upon sonicating both UV-exposed and unexposed films in DMF; the UV-unexposed films dissolve, while the exposed films remain intact (Figure S6).

A key advantage of using the UV-induced thiol−ene cross-linking approach is that it is possible to control the degree of cross-linking by the amount of exposure to UV irradiation.[48,49] As such, the imbibed P(VAc-*co*-VP_x)/*t*-CNC-COOH films (where x = 10, 22, or 30 wt %) were irradiated with UV light (60 mW/cm^2) for times ranging from 2 to 40 min. Prior studies have shown that the CNCs can scatter the UV light, limiting its penetration depth through the composite films during the photocuring process.[41] Thus, to ensure a more even distribution of UV exposure through the film's thickness, the samples were irradiated on both sides (films were flipped at the halfway point of exposure). Finally, the irradiated samples were swollen in 2-propanol for 24 h to remove unreacted initiator and cross-linker before being dried under reduced pressure for further characterization. A control sample (unexposed to UV light) was also prepared by directly washing the imbibed composite strip in 2-propanol followed by the same drying procedures.

The thermomechanical properties of these bioinspired nanocomposites were characterized by dynamic mechanical analysis (DMA) in both dry and wet states. Representative DMA temperature sweep curves showing the temperature dependency of storage modulus (E') and tan δ of P(VAc-*co*-VP_{30})/*t*-CNC-COOH nanocomposites in the dry state before and after UV irradiation are shown in Figure 1a. The storage modulus exhibits a transition between 30 and 60 °C, attributed to the glass transition temperature, T_g, of the P(VAc-*co*-VP) matrix and a rubbery plateau at higher temperatures. After UV irradiation, a shift of the tan δ peak to higher temperatures as the exposure time increases can be observed. For example, the tan δ peak of unexposed P(VAc-*co*-VP_{30})/*t*-CNC-COOH nanocomposites increased from about 43 to 58 °C after 40 min UV irradiation (Table 1), consistent with covalent cross-linking of the polymer matrix.[50] Similar behavior is also observed in the P(VAc-*co*-VP_{10})/*t*-CNC-COOH and P(VAc-*co*-VP_{22})/*t*-CNC-COOH nanocomposites (Figure S7). It is worthy of note that, in the first-generation of these bioinspired nanocomposites, in which cross-linking only occurs between the CNCs, there is no change in the T_g of the PVAc matrix after UV irradiation.[40,41]

The formation of covalent networks within the P(VAc-*co*-VP)/*t*-CNC-COOH nanocomposites can be further demonstrated by the increase in plateau storage modulus (E') after 2−40 min of UV irradiation. The plateau E' at 80 °C (ca. 20 °C higher than the highest T_g) were obtained from the DMA temperature sweep curves and used to evaluate the effect of UV irradiation condition on the mechanical properties. As can be seen from Figure 1b, all the nanocomposites showed an increase in E' (80 °C) with longer irradiation times. The composite samples fabricated using P(VAc-*co*-VP_{30}) demonstrate the highest plateau E' (>600 MPa) after 40 min irradiation (Table 1), consistent with a higher level of cross-linking in this material. In all samples there is a relatively small contrast in dry plateau storage modulus at 80 °C between uncross-linked (0 min, E'_{soft}) and cross-linked samples (40 min, E'_{stiff}). For example, P(VAc-*co*-VP_{30})/*t*-CNC-COOH nanocomposites have a E'_{stiff}/E'_{soft} = 1.6, slightly lower than the first-generation bioinspired nanocomposites based on filler−filler cross-links (E'_{stiff}/E'_{soft} = 2).

Of course, as it relates to the squid beak biomodel, what is more important for this class of materials is the mechanical properties of the wet composite films. In the wet state, a similar trend of increasing T_g and plateau modulus is observed after exposure to UV light for 2−40 min as can be seen from the representative DMA temperature sweep studies of the P(VAc-*co*-VP_{30})/*t*-CNC-COOH nanocomposites (Figure 2a). All the composite samples were preswollen in water until equilibrium swelling was reached before testing, and the DMA characterization was carried out in a submersion chamber. Compared to the dry films, a clear shift of the tan δ peak to lower temperatures can be observed in the wet materials, which is attributed to the water plasticization of the polymer matrix. For example, while the T_g for the unexposed P(VAc-*co*-VP_{30})/*t*-

https://dx.doi.org/10.1021/acs.biomac.0c01051
Biomacromolecules 2021, 22, 201−212

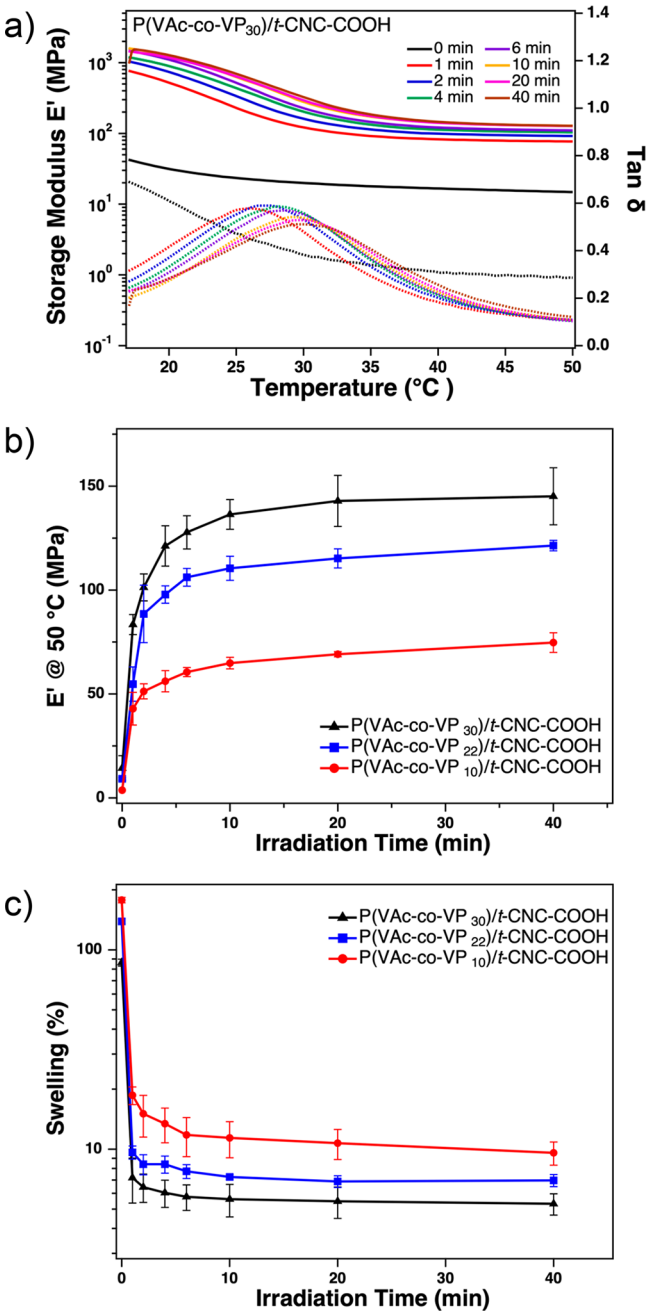

Figure 2. (a) Representative DMA temperature sweeps of P(VAc-*co*-VP_{30})/*t*-CNC-COOH nanocomposites in the wet state before and after UV irradiation. (b) Storage modulus, E', at 50 °C and (c) equilibrium water swelling of various P(VAc-*co*-VP)/*t*-CNC-COOH nanocomposites after different UV irradiation times ($N = 3$, error bars represent the standard deviation; DMA conditions: heating rate 3 °C/min, frequency 1 Hz, strain 0.1%).

CNC-COOH composites in the wet state is too low to be obtained from the DMA study, the T_g of the irradiated nanocomposite increased to about 30 °C after 40 min UV irradiation. This result is consistent with the successful cross-linking within the polymer matrix and is further supported by the fact the increase in T_g is related to the amount of alkene moieties within the nanocomposite; the P(VAc-*co*-VP_{22}) and P(VAc-*co*-VP_{10}) nanocomposites show a T_g increase from about 17 to 28 °C and from about 20 to 22 °C after 40 min UV irradiation, respectively (Figure S8).

Importantly, the wet plateau E' can be controlled by varying the UV irradiation time as well as the amount of cross-linkable groups in the matrix (Figure 2b). For the P(VAc-*co*-VP_{30})/*t*-CNC-COOH nanocomposites, samples irradiated for 40 min show a wet plateau E' of 145 MPa and in this material the wet modulus contrast, E'_{stiff}/E'_{soft}, between the irradiated and unexposed films is about 11. This compares to a contrast of about 7 with the PVAc/*t*-CNC-allyl nanocomposites, where cross-linking is predominantly occurring between the CNCs.[41]

Interestingly, the wet mechanical contrast does not change significantly in the composites that have a lower amount of alkene groups in the polymer matrix. Wet contrast values of about 12 and 13 are observed with the P(VAc-*co*-VP_{10}) and P(VAc-*co*-VP_{22}) composites, respectively. Although, of course, in these materials the maximum wet modulus is lower at 75 MPa for P(VAc-*co*-VP_{10}) and 121 MPa for P(VAc-*co*-VP_{22}) (Tables S3 and S4). A possible explanation is that while the wet E'_{stiff} is larger in the P(VAc-*co*-VP_{30}) composites on account of a higher cross-link density, the higher mole percent of VP units increases the hydrophobicity of the matrix which limits the E'_{soft} of the unexposed materials in the wet state (which is 5.4, 9.2, and 13.4 MPa for the P(VAc-*co*-VP_x) composites, where x = 10, 22, and 30, respectively). This increased hydrophobicity of the cross-linked matrix is seen in the degree of water swelling of the different composite systems (Figure 2c). The unexposed P(VAc-*co*-VP_{10}) nanocomposites with the least amount of VP moieties shows the highest amount of water uptake, about 180 wt %. Water swelling significantly decreases for the composites based on P(VAc-*co*-VP_{22}) (ca. 140 wt %) and P(VAc-*co*-VP_{30}) (ca. 85 wt %). All the composite samples displayed a dramatic decrease in water uptake after UV irradiation which is again consistent with the formation of thiol−ene cross-linked networks. It is worthwhile noting that the water uptake for all these composite samples after 40 min of irradiation is between 5 to 10 wt %, which is significantly lower than is observed for the first-generation bioinspired cross-linked nanocomposites based on PVAc/*t*-CNC-allyl-COOH, whose swelling was greater than 20 wt %.[41]

Nanocomposites Fabricated by Cross-Linking both the Polymer Matrix and CNC Fillers. The above data shows that it is possible to access bioinspired, controlled wet modulus nanocomposites, with mechanical contrast >10 and stiff wet modulus >140 MPa, by cross-linking of the matrix. It was therefore of interest to investigate if the wet mechanical properties of the CNC based nanocomposites can be further enhanced by introducing cross-linking between the matrix and the CNCs, as well as within the matrix and between the CNCs. To this end, nanocomposites were fabricated using allyl-functionalized CNCs (*t*-CNC-allyl-COOH, Scheme 2b) as fillers embedded in the P(VAc-*co*-VP_x) copolymer matrices investigated above. It is important to note that the addition of the allyl-CNCs further increases the number of cross-linking sites in the composite, as discussed above 15 wt % *t*-CNC-allyl-COOH contributes to 0.12×10^{-3} mmol/kg of alkene moieties in the nanocomposites. A comparison of the total alkene content (in mmol/mg) of the different nanocomposites is summarized in Table 2. Films were cast and imbibed under the same conditions as described previously with the amount of PETMP cross-linkers adjusted based on the total amount of alkene units (on both the *t*-CNC-allyl-COOH nanofillers (800 mmol/kg) and the P(VAc-*co*-VP) matrix) to maintain a 1:1 thiol to alkene molar ratio. Covalent thiol−ene networks between the CNCs and the polymer matrix were formed by

https://dx.doi.org/10.1021/acs.biomac.0c01051
Biomacromolecules 2021, 22, 201−212

Table 2. Comparison of the Content of Alkene Moieties in Nanocomposites

sample	cross-link type	filler content (wt %)	[alkene] from CNC (mmol/mg)	[alkene] from polymer (mmol/mg)	total [alkene] (mmol/mg)
PVAc/*t*-CNC-allyl	filler−filler	15	0.12×10^{-3}	0	0.12×10^{-3}
P(VAc-*co*-VP_{10})/*t*-CNC-COOH	matrix−matrix	15	0	0.94×10^{-3}	0.94×10^{-3}
P(VAc-*co*-VP_{22})/*t*-CNC-COOH	matrix−matrix	15	0	1.99×10^{-3}	1.99×10^{-3}
P(VAc-*co*-VP_{30})/*t*-CNC-COOH	matrix−matrix	15	0	2.60×10^{-3}	2.60×10^{-3}
P(VAc-*co*-VP_{10})/ *t*-CNC-allyl-COOH	matrix−filler	15	0.12×10^{-3}	0.94×10^{-3}	1.06×10^{-3}
P(VAc-*co*-VP_{22})/ *t*-CNC-allyl-COOH	matrix−filler	15	0.12×10^{-3}	1.99×10^{-3}	2.11×10^{-3}
P(VAc-*co*-VP_{30})/ *t*-CNC-allyl-COOH	matrix−filler	15	0.12×10^{-3}	2.60×10^{-3}	2.72×10^{-3}

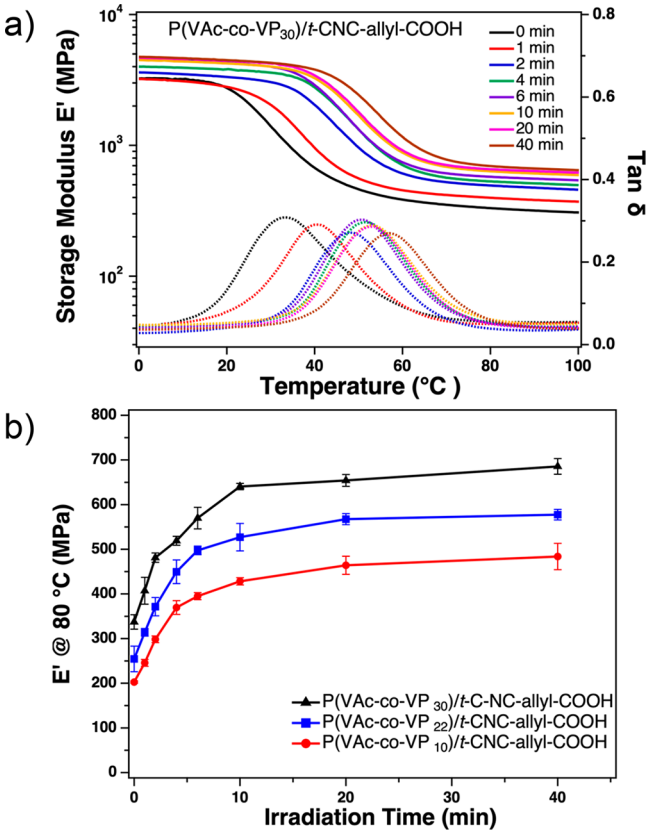

Figure 3. (a) Representative DMA temperature sweep study of P(VAc-*co*-VP_{30})/*t*-CNC-allyl-COOH nanocomposites in the dry state before and after UV irradiation. (b) Storage modulus E' at 80 °C of various P(VAc-*co*-VP)/*t*-CNC-allyl-COOH nanocomposites at different UV irradiation times (N = 3, error bars represent the standard deviation; DMA conditions: heating rate 3 °C/min, frequency 1 Hz, strain 0.1%).

irradiating the composite films with UV light using the same conditions as discussed above (60 mW/cm^2, 2−40 min). Similar to the nanocomposites made with *t*-CNC-COOH, the successful cross-linking was initially confirmed by DMF solubility tests using unexposed and cross-linked P(VAc-*co*-VP_{30})/*t*-CNC-allyl-COOH nanocomposites (Figure S9). Consistent with cross-linking, the sample irritated for 40 min remained intact after swelling and sonication in DMF, as compared to the unexposed showing a complete dissolution in DMF.

DMA temperature sweep studies of P(VAc-*co*-VP_{30})/*t*-CNC-allyl-COOH nanocomposites before and after UV irradiation in the dry state are shown in Figure 3a. In the dry state, the general shapes of the storage modulus (E') and tan δ curves of the P(VAc-*co*-VP)/*t*-CNC-allyl-COOH films are similar to the composites containing the *t*-CNC-COOH fillers. A shift of the tan δ peak to higher temperatures (38.0−54.5 °C) and an increase of the plateau storage modulus (337−686 MPa at 80 °C) of the samples irradiated for 40 min can be observed (Table 3). It is worthy of note that both the tan δ peak (38.0 °C) and plateau modulus (337 MPa) for unexposed P(VAc-*co*-VP_{30})/*t*-CNC-allyl-COOH films are lower relative to P(VAc-*co*-VP_{30})/*t*-CNC-COOH composite films (43.4 °C and 385 MPa), possibly on account of reduced filler−filler and filler−matrix (hydrogen bonding) interactions that occur as a result of the functionalization the CNCs surface with allyl groups.

After irradiation for 40 min, the plateau modulus (above T_g) for P(VAc-*co*-VP_{30})/*t*-CNC-allyl-COOH nanocomposite increased to about 686 ± 18 MPa, which is slightly improved compared to P(VAc-*co*-VP_{30})/*t*-CNC-COOH (ca. 612 ± 21 MPa). The result is presumably a consequence of the additional degree of cross-linking between the filler and matrix, as well as between CNC fillers.

As mentioned in the study above, the wet mechanical properties of these films are of more interest given the squid beak exhibits its mechanical gradient in wet conditions. Representative submersion DMA curves of P(VAc-*co*-VP_{30})/*t*-CNC-allyl-COOH films after different periods of UV irradiation are shown in Figure 4a (DMA curves of P(VAc-*co*-VP_{22})/*t*-CNC-allyl-COOH and P(VAc-*co*-VP_{10})/*t*-CNC-allyl-COOH are shown in Figure S11). Relative to the nanocomposites with covalent cross-links only within the matrix, the introduction of the additional matrix−filler/filler−filler cross-links yields an increase in both the T_g, as well as plateau modulus after UV irradiation. For example, the T_g of P(VAc-*co*-VP_{30})/*t*-CNC-allyl-COOH increased to about 34 °C after 40 min UV irradiation (cf. ca. 30 °C for P(VAc-*co*-VP_{30})/*t*-CNC-COOH), while the plateau E' increased to about 200 MPa at 50 °C (cf. ca. 130 MPa for P(VAc-*co*-VP_{30})/*t*-CNC-COOH at 50 °C). As a result, the wet modulus contrast before and after UV irradiation is improved (E'_{stiff}/E'_{soft} = ca. 16) for P(VAc-*co*-VP_{30})/*t*-CNC-allyl-COOH nanocomposites. The same trend can also be observed in the other two nanocomposites with matrices containing a lower mole fraction of pendant alkene groups (Figure 4b). The wet plateau E' rose from 9 to 126 MPa for P(VAc-*co*-VP_{22})/*t*-CNC-allyl-COOH (E'_{stiff}/E'_{soft} = ca. 14) upon UV irradiation, while the contrast for P(VAc-*co*-VP_{10})/*t*-CNC-allyl-COOH is from 5 to 80 MPa with a E'_{stiff}/E'_{soft} of about 15. Using the combination of the allyl-functionalized CNC with the alkene-containing polymer matrix does result in an increase in the wet plateau modulus of

https://dx.doi.org/10.1021/acs.biomac.0c01051
Biomacromolecules 2021, 22, 201−212

Table 3. Summary of the Thermal Mechanical Properties of P(VAc-*co*-VP_{30})/*t*-CNC-allyl-COOH in Both the Dry and Wet States at Different UV Irradiation Times (N = 3, Errors are Standard Deviation)[a]

	P(VAc-*co*-VP_{30})/*t*-CNC-allyl-COOH				
irradiation time (min)	dry E' at 80 °C (MPa)	dry T_g (°C)	wet E' at 50 °C (MPa)	wet T_g (°C)	water swelling (%)
0	337 ± 16	38.0 ± 5.8	12.7 ± 4		61.2 ± 6.0
1	407 ± 30	42.8 ± 4.8	103 ± 6	26.0 ± 1.2	7.1 ± 1.0
2	481 ± 10	47.2 ± 3.4	118 ± 8	28.1 ± 1.0	5.7 ± 0.7
4	519 ± 10	48.6 ± 3.6	139 ± 4	29.2 ± 0.5	5.6 ± 0.5
6	570 ± 24	49.7 ± 2.6	146 ± 6	30.1 ± 0.4	4.8 ± 0.2
10	641 ± 7	50.3 ± 3.9	155 ± 7	30.9 ± 1.5	4.9 ± 0.1
20	654 ± 13	51.7 ± 1.3	177 ± 11	33.3 ± 1.1	4.7 ± 0.2
40	686 ± 18	54.5 ± 2.1	197 ± 4	33.5 ± 1.1	4.2 ± 0.4

[a]All data are based on DMA experiments.

the highly cross-linked materials (E'_{stiff}), but, akin to what is observed for the P(VAc-*co*-VP)/*t*-CNC-COOH nanocomposites, the overall contrast is limited by a slightly higher E'_{soft} of the unexposed materials on account of the increased hydrophobicity of both the filler and matrix.

The equilibrium water swelling of the nanocomposite films containing cross-links between matrix and filler before and after UV irradiation are shown in Figure 4c. As expected, the equilibrium water uptake drops dramatically as the UV irradiation time increases, which is consistent with the formation of covalent cross-links. The equilibrium water uptake for these allyl-functionalized CNC composites is decreased to 4−7% relative to the 5−10% for films containing CNC-COOHs, which is presumably the consequence of the more hydrophobic (allyl) moieties on the CNCs surface.

While the above-mentioned mechanical contrasts are all calculated based on the modulus in the plateau region at 50 °C, it is worthwhile pointing out that at physiological temperature (37 °C) the modulus contrast (E'_{stiff}/E'_{soft}) is about 20, with a tunable E' between 14 and 289 MPa, depending on the degree of irradiation. Such bioinspired nanocomposites with improved wet modulus contrast could facilitate the design of novel intracortical microelectrodes.[23,37,38]

Figure 5a compares the wet storage modulus vs irradiation time for the three classes of CNC-based nanocomposites that differ in both the degree and type of cross-linking (between the CNCs, within the matrix or cross-linking of the matrix and CNCs). The data demonstrate that nanocomposites containing matrix−fillers cross-links (and the higher degree of cross-linking) show higher plateau E' after UV irradiation compared to composites containing only matrix−matrix or filler−filler cross-links. Of course, the P(VAc-*co*-VP_{30}) nanocomposites contain a much higher content of alkene moieties relative to the PVAc-based materials (CNC−CNC cross-links only; Table 2). Therefore, the lower wet modulus in the filler-only cross-link material is presumably a consequence of the limited number of cross-linking sites within the nanocomposites. For comparison, Figure 5b and c show the wet modulus (E') and degree of water swelling (after the maximum amount of UV exposure) versus the alkene moiety content in the pre-cross-linked films for the six films reported in this study and the previously reported PVAc/*t*-CNC-allyl-COOH. In general, as would be expected, the higher the alkene content the higher the wet modulus and the lower the degree of swelling after cross-linking. While it is difficult to draw too many other conclusions from this data it is worthwhile pointing out that, even though the total alkene content in P(VAc-*co*-VP_{30})/*t*-CNC-allyl-COOH (matrix−filler) is only slightly higher than P(VAc-*co*-VP_{30})/*t*-CNC-COOH (matrix−matrix; ca. 4.6 mol % increase), the wet mechanical properties show about 36% increase in the wet E'_{stiff} for these highly cross-linked samples.

Photopatterning of Bioinspired Nanocomposites. One advantage of using a photoinduced cross-linking approach is the ability to photopattern the materials using a predesigned photomask. For example, Kumacheva and co-workers have shown that a hydrogel sheet containing alternating stripe patterns of different cross-linked poly(NIPAm)/poly(AMPS) after photopatterning can transform into a 3D helical shape when placed in hot water or a NaCl solution on account of the variation in the degree of water swelling between the exposed and unexposed regions.[51] In addition, they showed that the pitch of the helix is proportional to the tilt (tan θ) of the stripes. Thus, to examine if these bioinspired nanocomposite films had a similar capability they were photopatterned using a mask. A P(VAc-*co*-VP_{30})/*t*-CNC-allyl-COOH nanocomposite film (30 mm × 4 mm) was chosen as an example and was irradiated with UV using a photomask for 20 min on only one side of the sample. The photomask contains alternating dark and transparent strips that are 1 mm in width, and are tilted at a given angle to the long axis of the film (either 30° or 60°; Figure 6a). This procedure aims to transfer the strip patterns to the nanocomposites to create alternating cross-linked (under transparent mask areas) and un-cross-linked regions (under dark mask areas) with different mechanical properties and degrees of swelling. After UV irradiation, the composite samples were placed in DCM, and the film transformed into a helical 3D structure within a few minutes (Figure 6b,c). The shape transformation is presumably a result of the difference in swelling between the cross-linked and un-cross-linked regions. Consistent with the work of Kumacheva[51] the morphology of the helix did depend on the angle of the pattern, with a more compacted helical structure formed at a smaller angle (30°). It can be expected that with the use of nanofabrication equipment and a properly designed and fabricated photomask, more complex patterns and shapes can be fabricated which broadens the application of these bioinspired nanocomposites.

CONCLUSIONS

Building on our previous squid beak inspired nanocomposites prepared with allyl-functionalized CNCs embedded in a PVAc matrix, a next-generation of bioinspired nanocomposites have been prepared and investigated using a cross-linkable alkene-containing poly(vinyl acetate-*co*-vinyl pentenoate) P(VAc-*co*-VP) copolymer matrix. Both P(VAc-*co*-VP)/*t*-CNC-COOH and P(VAc-*co*-VP)/*t*-CNC-allyl-COOH nanocomposites were

https://dx.doi.org/10.1021/acs.biomac.0c01051
Biomacromolecules 2021, 22, 201−212

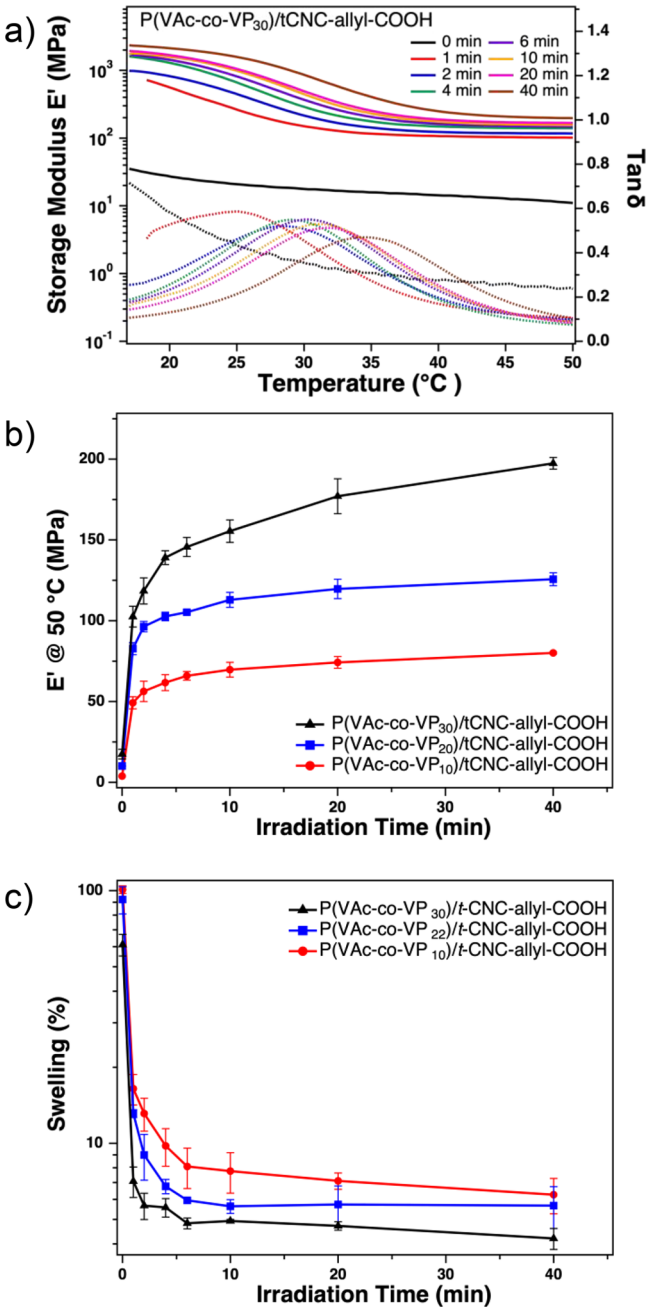

Figure 4. (a) Representative DMA temperature sweeps of P(VAc-*co*-VP_{30})/*t*-CNC-allyl-COOH nanocomposites in the wet state before and after UV irradiation. (b) Storage modulus E' at 50 °C and (c) equilibrium water swelling of various P(VAc-*co*-VP)/*t*-CNC-allyl-COOH nanocomposites at different UV irradiation times (N = 3, error bars represent the standard deviation; DMA conditions: heating rate 3 °C/min, frequency 1 Hz, strain 0.1%).

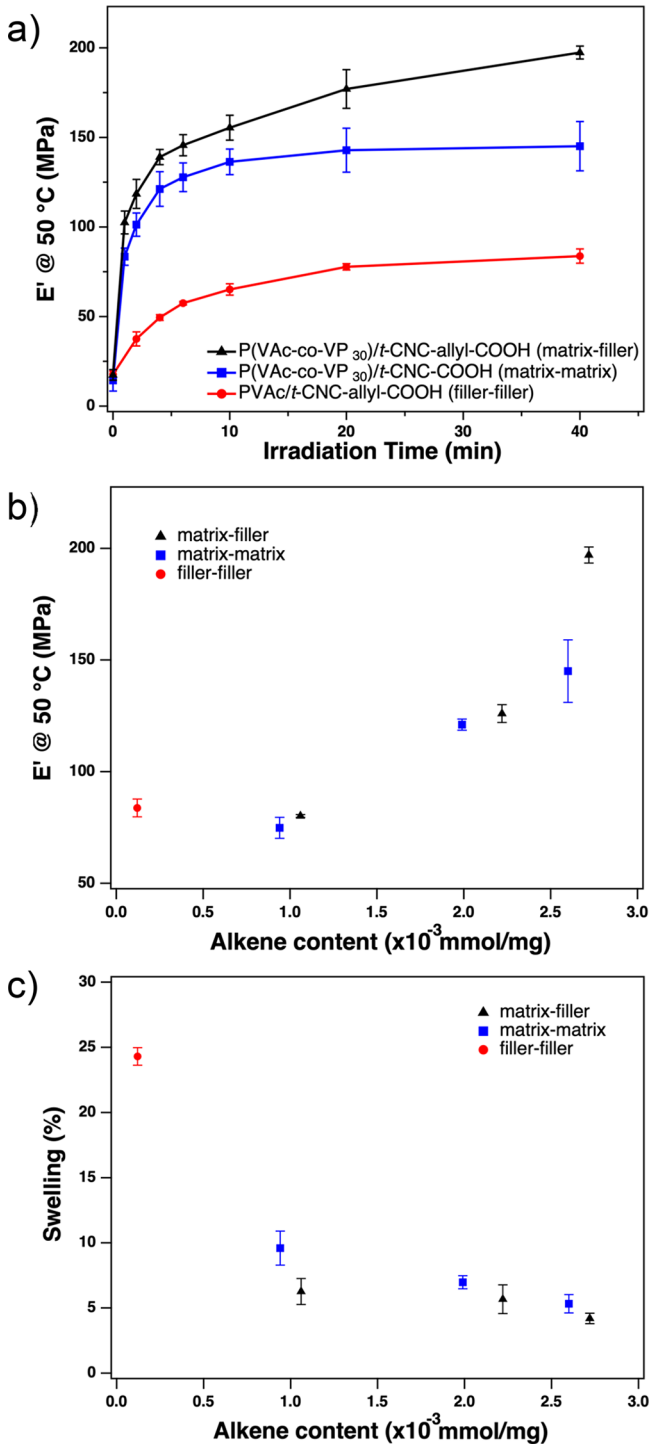

Figure 5. (a) Comparison of the wet storage modulus E' at 50 °C of PVAc/*t*-CNC-allyl-COOH,[41] P(VAc-*co*-VP_{30})/*t*-CNC-COOH, and P(VAc-*co*-VP_{30})/*t*-CNC-allyl-COOH. (b) Comparison of the wet storage modulus E' and (c) degree of swelling at 50 °C of the different 15 wt % CNC bioinspired nanocomposites with filler−filler cross-linking (PVAc/*t*-CNC-allyl-COOH), matrix−matrix cross-linking (P(VAc-*co*-VP_x)/*t*-CNC-COOH, x = 10, 22, and 30) and matrix−filler (P(VAc-*co*-VP_x)/*t*-CNC-allyl-COOH, x = 10, 22, and 30) in the pre-cross-linked films.

prepared, and the materials can be covalently cross-linked using photoinduced thiol−ene chemistry to yield composite films. By using a polymer matrix with pendant alkene groups, the covalent network formed by photoinduced thiol−ene chemistry can be further extended to include matrix−matrix and matrix−filler cross-links, which improves both the wet stiffness and wet modulus contrast of the nanocomposite films compared to the first-generation filler only cross-linked composite films. Specifically, nanocomposites composed of 15 wt % *t*-CNC-allyl-COOH and P(VAc-*co*-VP_{30}) (matrix−filler cross-links) with about 30 mol % of alkene-containing repeat units exhibited a wet storage modulus at 50 °C that is tunable between 13 MPa (un-cross-linked) and 197 MPa after 40 min of UV cross-linking (E'_{stiff}/E'_{soft} = ca. 16). The contrast

https://dx.doi.org/10.1021/acs.biomac.0c01051
Biomacromolecules 2021, 22, 201−212

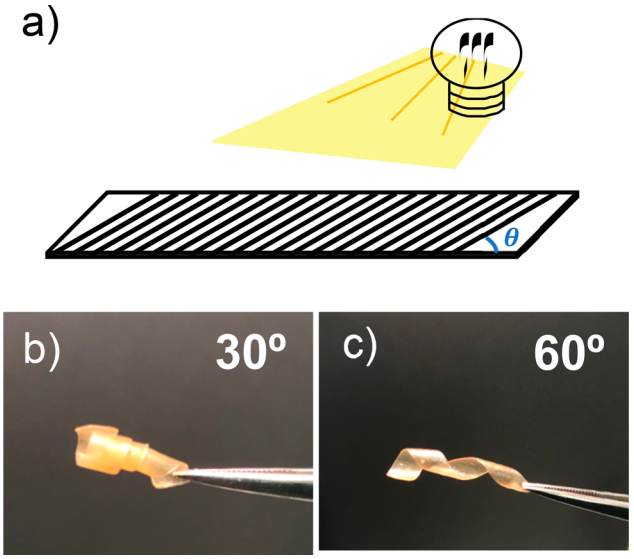

Figure 6. (a) Schematic representation of the photomasks. (b, c) Photos of the P(VAc-*co*-VP_{30})/*t*-CNC-allyl-COOH nanocomposites after irradiation under a photomask and swelled in DCM for 5 min. The labels on b and c show the angle of the strip patters to the long axis.

in wet modulus is slightly higher relative to the matrix cross-linked nanocomposites containing 15 wt % *t*-CNC-COOH and P(VAc-*co*-VP_{30}), which have a E'_{stiff}/E'_{soft} = ca. 11 (13−145 MPa). It is also worthwhile pointing out that at physiological temperature (37 °C), the wet composites of *t*-CNC-allyl-COOH and P(VAc-*co*-VP_{30}) (matrix−filler cross-link) demonstrate an even larger modulus contrast at E'_{stiff}/E'_{soft} = ca. 20 (between 289 and 14 MPa), which is much higher relative to what was obtained in the original work (E'_{stiff}/E'_{soft} = ca. 7).[41] Preliminary studies on the photopatterning of these composite films have shown that it is also possible to control the mechanical properties and swelling behavior within different regions of the materials by using a photomask, which opens the door to fabrication of these materials with complex shapes or even with spatial mechanical gradients.

■ ASSOCIATED CONTENT

Supporting Information

The Supporting Information is available free of charge at https://pubs.acs.org/doi/10.1021/acs.biomac.0c01051.

^{1}H NMR (500 MHz, $CDCl_3$) spectra of P(VAc-*co*-VA) copolymer and P(VAc-*co*-VP) copolymer; ^{1}H NMR (500 MHz, $CDCl_3$) spectra of 4-pentenoyl chloride; FTIR of PVAc, P(VAc-*co*-VA) and P(VAc-*co*-VP); DSC of P(VAc-*co*-VP) copolymer with various amount of VP units; swelling test of P(VAc-*co*-VP_{30})/*t*-CNC-COOH nanocomposites in DMF before and after UV irradiation; DMA temperature sweep of P(VAc-*co*-VP_{10})/*t*-CNC-COOH and P(VAc-*co*-VP_{22})/*t*-CNC-COOH nanocomposites in the dry and wet state; summary of the thermal mechanical property of P(VAc-*co*-VP_{10})/*t*-CNC-COOH and P(VAc-*co*-VP_{22})/*t*-CNC-COOH nanocomposites; swelling test of P(VAc-*co*-VP_{30})/*t*-CNC-allyl-COOH nanocomposites in DMF before and after UV irradiation; DMA temperature sweep study of P(VAc-*co*-VP_{10})/*t*-CNC-allyl-COOH and (VAc-*co*-VP_{22})/*t*-CNC-allyl-COOH nanocomposites in the dry and wet state; summary of the thermal mechanical property of P(VAc-*co*-VP_{10})/*t*-CNC-allyl-COOH and P(VAc-*co*-VP_{22})/*t*-CNC-allyl-COOH nanocomposites (PDF)

■ AUTHOR INFORMATION

Corresponding Author

Stuart J. Rowan − *Pritzker School of Molecular Engineering and Department of Chemistry, University of Chicago, Chicago, Illinois 60637, United States; Chemical and Engineering Sciences, Argonne National Laboratory, Lemont, Illinois 60439, United States;* orcid.org/0000-0001-8176-0594; Email: stuartrowan@uchicago.edu

Authors

Yefei Zhang − *Pritzker School of Molecular Engineering, University of Chicago, Chicago, Illinois 60637, United States*

Nanetta Pon − *Department of Chemistry, University of Chicago, Chicago, Illinois 60637, United States*

Ahmed Awaji − *Department of Macromolecular Science and Engineering, Case Western Reserve University, Cleveland, Ohio 44106, United States*

Complete contact information is available at: https://pubs.acs.org/10.1021/acs.biomac.0c01051

Notes

The authors declare no competing financial interest.

■ ACKNOWLEDGMENTS

This project is supported by the National Science Foundation under Grant No. NSF #1204948, the National Science Foundation PIRE program under Grant No. NSF #1743475, and the Pritzker School of Molecular Engineering at the University of Chicago. Part of this work was carried out using the Soft Matter Characterization Facility of the University of Chicago. This work made use of the shared facilities at the University of Chicago Materials Research Science and Engineering Center, supported by National Science Foundation under Award Number DMR-1420709.

■ REFERENCES

(1) Dunlop, J. W. C.; Fratzl, P. Biological Composites. *Annu. Rev. Mater. Res.* **2010**, *40* (1), 1−24.

(2) Vincent, J. F. V. Biomimetic Materials. *J. Mater. Res.* **2008**, *23* (12), 3140−3147.

(3) Wegst, U. G. K.; Ashby, M. F. The Mechanical Efficiency of Natural Materials. *Philos. Mag.* **2004**, *84* (21), 2167−2186.

(4) Chen, P.-Y.; McKittrick, J.; Meyers, M. A. Biological Materials: Functional Adaptations and Bioinspired Designs. *Prog. Mater. Sci.* **2012**, *57* (8), 1492−1704.

(5) Sun, J.; Bhushan, B. Hierarchical Structure and Mechanical Properties of Nacre: A Review. *RSC Adv.* **2012**, *2* (20), 7617.

(6) Motokawa, T.; Tsuchi, A. Dynamic Mechanical Properties of Body-Wall Dermis in Various Mechanical States and Their Implications for the Behavior of Sea Cucumbers. *Biol. Bull.* **2003**, *205* (3), 261−275.

(7) Koob, T. J.; Koob-Emunds, M. M.; Trotter, J. A. Cell-Derived Stiffening and Plasticizing Factors in Sea Cucumber (Cucumaria Frondosa) Dermis. *J. Exp. Biol.* **1999**, *202* (17), 2291−2301.

(8) Szulgit, G. K.; Shadwick, R. E. Dynamic Mechanical Characterization of a Mutable Collagenous Tissue: Response of Sea Cucumber Dermis to Cell Lysis and Dermal Extracts. *J. Exp. Biol.* **2000**, *203* (10), 1539−1550.

(9) Weaver, J. C.; Milliron, G. W.; Miserez, A.; Evans-Lutterodt, K.; Herrera, S.; Gallana, I.; Mershon, W. J.; Swanson, B.; Zavattieri, P.; DiMasi, E.; Kisailus, D. The Stomatopod Dactyl Club: A Formidable Damage-Tolerant Biological Hammer. *Science* **2012**, *336* (6086), 1275−1280.
(10) Amini, S.; Tadayon, M.; Idapalapati, S.; Miserez, A. The Role of Quasi-Plasticity in the Extreme Contact Damage Tolerance of the Stomatopod Dactyl Club. *Nat. Mater.* **2015**, *14* (9), 943−950.
(11) Zhao, Y.; Cao, J.; Zhang, Y.; Peng, H. Gradually Crosslinking Carbon Nanotube Array in Mimicking the Beak of Giant Squid for Compression-Sensing Supercapacitor. *Adv. Funct. Mater.* **2020**, *30*, 1902971.
(12) Bai, J.; Shi, Z.; Yin, J.; Tian, M.; Qu, R. Shape Reconfiguration of a Biomimetic Elastic Membrane with a Switchable Janus Structure. *Adv. Funct. Mater.* **2018**, *28* (29), 1800939.
(13) Zhao, Z.; Fang, R.; Rong, Q.; Liu, M. Bioinspired Nanocomposite Hydrogels with Highly Ordered Structures. *Adv. Mater.* **2017**, *29* (45), 1703045.
(14) Thompson, C. B.; Chatterjee, S.; Korley, L. T. J. Gradient Supramolecular Interactions and Tunable Mechanics in Polychaete Jaw Inspired Semi-Interpenetrating Networks. *Eur. Polym. J.* **2019**, *116*, 201−209.
(15) Montero de Espinosa, L.; Meesorn, W.; Moatsou, D.; Weder, C. Bioinspired Polymer Systems with Stimuli-Responsive Mechanical Properties. *Chem. Rev.* **2017**, *117* (20), 12851−12892.
(16) Wegst, U. G. K.; Bai, H.; Saiz, E.; Tomsia, A. P.; Ritchie, R. O. Bioinspired Structural Materials. *Nat. Mater.* **2015**, *14* (1), 23−36.
(17) Zhang, C.; Mcadams, D. A.; Grunlan, J. C. Nano/Micro-Manufacturing of Bioinspired Materials: A Review of Methods to Mimic Natural Structures. *Adv. Mater.* **2016**, *28* (30), 6292−6321.
(18) Zhou, B. Bio-Inspired Study of Structural Materials. *Mater. Sci. Eng., C* **2000**, *11* (1), 13−18.
(19) Zhao, H.; Yang, Z.; Guo, L. Nacre-Inspired Composites with Different Macroscopic Dimensions: Strategies for Improved Mechanical Performance and Applications. *NPG Asia Mater.* **2018**, *10* (4), 1−22.
(20) Ortiz, C.; Boyce, M. C. MATERIALS SCIENCE: Bioinspired Structural Materials. *Science* **2008**, *319* (5866), 1053−1054.
(21) Jacucci, G.; Schertel, L.; Zhang, Y.; Yang, H.; Vignolini, S. Light Management with Natural Materials: From Whiteness to Transparency. *Adv. Mater.* **2020**, *2001215*, 2001215.
(22) Wang, Z.; Wang, K.; Huang, H.; Cui, X.; Shi, X.; Ma, X.; Li, B.; Zhang, Z.; Tang, X.; Chiang, M. Y. M. Bioinspired Wear-Resistant and Ultradurable Functional Gradient Coatings. *Small* **2018**, *14* (41), 1802717.
(23) Nguyen, J. K.; Park, D. J.; Skousen, J. L.; Hess-Dunning, A. E.; Tyler, D. J.; Rowan, S. J.; Weder, C.; Capadona, J. R. Mechanically-Compliant Intracortical Implants Reduce the Neuroinflammatory Response. *J. Neural Eng.* **2014**, *11* (5), 056014.
(24) Chen, C.; Liu, D.; He, L.; Qin, S.; Wang, J.; Razal, J. M.; Kotov, N. A.; Lei, W. Bio-Inspired Nanocomposite Membranes for Osmotic Energy Harvesting. *Joule* **2020**, *4* (1), 247−261.
(25) Miserez, A.; Schneberk, T.; Sun, C.; Zok, F. W.; Waite, J. H. The Transition from Stiff to Compliant Materials in Squid Beaks. *Science* **2008**, *319* (5871), 1816−1819.
(26) Miserez, A.; Li, Y.; Waite, J. H.; Zok, F. Jumbo Squid Beaks: Inspiration for Design of Robust Organic Composites. *Acta Biomater.* **2007**, *3* (1), 139−149.
(27) Miserez, A.; Rubin, D.; Waite, J. H. Cross-Linking Chemistry of Squid Beak. *J. Biol. Chem.* **2010**, *285* (49), 38115−38124.
(28) Cai, H.; Gabryelczyk, B.; Manimekalai, M. S. S.; Grüber, G.; Salentinig, S.; Miserez, A. Self-Coacervation of Modular Squid Beak Proteins − a Comparative Study. *Soft Matter* **2017**, *13* (42), 7740−7752.
(29) Tan, Y.; Hoon, S.; Guerette, P. A.; Wei, W.; Ghadban, A.; Hao, C.; Miserez, A.; Waite, J. H. Infiltration of Chitin by Protein Coacervates Defines the Squid Beak Mechanical Gradient. *Nat. Chem. Biol.* **2015**, *11* (7), 488−495.
(30) Zvarec, O.; Purushotham, S.; Masic, A.; Ramanujan, R. V.; Miserez, A. Catechol-Functionalized Chitosan/Iron Oxide Nanoparticle Composite Inspired by Mussel Thread Coating and Squid Beak Interfacial Chemistry. *Langmuir* **2013**, *29* (34), 10899−10906.
(31) Zhang, X.; Hassanzadeh, P.; Miyake, T.; Jin, J.; Rolandi, M. Squid Beak Inspired Water Processable Chitosan Composites with Tunable Mechanical Properties. *J. Mater. Chem. B* **2016**, *4* (13), 2273−2279.
(32) Neal, J. A.; Oldenhuis, N. J.; Novitsky, A. L.; Samson, E. M.; Thrift, W. J.; Ragan, R.; Guan, Z. Large Continuous Mechanical Gradient Formation via Metal-Ligand Interactions. *Angew. Chem., Int. Ed.* **2017**, *56* (49), 15575−15579.
(33) Claussen, K. U.; Giesa, R.; Schmidt, H.-W. Longitudinal Polymer Gradient Materials Based on Crosslinked Polymers. *Polymer* **2014**, *55* (1), 29−38.
(34) Wang, D.; Zhang, H.; Guo, J.; Cheng, B.; Cao, Y.; Lu, S.; Zhao, N.; Xu, J. Biomimetic Gradient Polymers with Enhanced Damping Capacities. *Macromol. Rapid Commun.* **2016**, *37* (7), 655−661.
(35) Fleckman, P.; Olerud, J. E. Models for the Histologic Study of the Skin Interface with Percutaneous Biomaterials. *Biomed. Mater.* **2008**, *3* (3), 034006.
(36) Lu, H. H.; Thomopoulos, S. Functional Attachment of Soft Tissues to Bone: Development, Healing, and Tissue Engineering. *Annu. Rev. Biomed. Eng.* **2013**, *15* (1), 201−226.
(37) Jorfi, M.; Skousen, J. L.; Weder, C.; Capadona, J. R. Progress towards Biocompatible Intracortical Microelectrodes for Neural Interfacing Applications. *J. Neural Eng.* **2015**, *12* (1), 011001.
(38) Shoffstall, A. J.; Capadona, J. R. Bioinspired Materials and Systems for Neural Interfacing. *Curr. Opin. Biomed. Eng.* **2018**, *6*, 110−119.
(39) Capadona, J. R.; Tyler, D. J.; Zorman, C. A.; Rowan, S. J.; Weder, C. Mechanically Adaptive Nanocomposites for Neural Interfacing. *MRS Bull.* **2012**, *37* (6), 581−589.
(40) Fox, J. D.; Capadona, J. R.; Marasco, P. D.; Rowan, S. J. Bioinspired Water-Enhanced Mechanical Gradient Nanocomposite Films That Mimic the Architecture and Properties of the Squid Beak. *J. Am. Chem. Soc.* **2013**, *135* (13), 5167−5174.
(41) Zhang, Y.; Edelbrock, A. N.; Rowan, S. J. Effect of Processing Conditions on the Mechanical Properties of Bio-Inspired Mechanical Gradient Nanocomposites. *Eur. Polym. J.* **2019**, *115*, 107−114.
(42) Biyani, M. V.; Jorfi, M.; Weder, C.; Foster, E. J. Light-Stimulated Mechanically Switchable, Photopatternable Cellulose Nanocomposites. *Polym. Chem.* **2014**, *5* (19), 5716−5724.
(43) Parambath Kanoth, B.; Claudino, M.; Johansson, M.; Berglund, L. A.; Zhou, Q. Biocomposites from Natural Rubber: Synergistic Effects of Functionalized Cellulose Nanocrystals as Both Reinforcing and Cross-Linking Agents via Free-Radical Thiol-Ene Chemistry. *ACS Appl. Mater. Interfaces* **2015**, *7* (30), 16303−16310.
(44) Blanchard, R.; Ogunsona, E. O.; Hojabr, S.; Berry, R.; Mekonnen, T. H. Synergistic Cross-Linking and Reinforcing Enhancement of Rubber Latex with Cellulose Nanocrystals for Glove Applications. *ACS Appl. Polym. Mater.* **2020**, *2* (2), 887−898.
(45) Park, J. W.; Im, S. S. Miscibility and Morphology in Blends of Poly(L-Lactic Acid) and Poly(Vinyl Acetate-Co-Vinyl Alcohol). *Polymer* **2003**, *44* (15), 4341−4354.
(46) Isasi, J. R.; Cesteros, L. C.; Katime, I. Hydrogen Bonding and Sequence Distribution in Poly(Vinyl Acetate-Co-Vinyl Alcohol) Copolymers. *Macromolecules* **1994**, *27* (8), 2200−2205.
(47) Ding, N.; Shentu, B.; Pan, P.; Shan, G.; Bao, Y.; Weng, Z. Synthesis and Crystallization of Poly(Vinyl Acetate)- g -Poly(l -Lactide) Graft Copolymer with Controllable Graft Density. *Ind. Eng. Chem. Res.* **2013**, *52* (36), 12897−12905.
(48) An, S. Y.; Lee, D. G.; Hwang, J. W.; Kim, K. N.; Nam, J. H.; Jung, H. W.; Noh, S. M.; Oh, J. K. Photo-Induced Thiol-Ene Polysulfide-Crosslinked Materials with Tunable Thermal and Mechanical Properties. *J. Polym. Sci., Part A: Polym. Chem.* **2014**, *52* (21), 3060−3068.
(49) Wiley, K. L.; Ovadia, E. M.; Calo, C. J.; Huber, R. E.; Kloxin, A. M. Rate-Based Approach for Controlling the Mechanical Properties of

https://dx.doi.org/10.1021/acs.biomac.0c01051
Biomacromolecules 2021, 22, 201−212

"thiol-Ene" Hydrogels Formed with Visible Light. *Polym. Chem.* **2019**, *10* (32), 4428−4440.
(50) Menard, K. P.; Menard, N. Dynamic Mechanical Analysis. In *Encyclopedia of Analytical Chemistry*; John Wiley & Sons, Ltd: Chichester, U.K., 2017; pp 1−25, DOI: 10.1002/9780470027318.a2007.pub3.
(51) Wu, Z. L.; Moshe, M.; Greener, J.; Therien-Aubin, H.; Nie, Z.; Sharon, E.; Kumacheva, E. Three-Dimensional Shape Transformations of Hydrogel Sheets Induced by Small-Scale Modulation of Internal Stresses. *Nat. Commun.* **2013**, *4* (1), 1586.

https://dx.doi.org/10.1021/acs.biomac.0c01051
Biomacromolecules 2021, 22, 201−212